Subsurface Imaging Using TEM Sounding Data

Guoqiang Xue[1], E. A. Elzein Mohammed[2], Xiu Li[3], Wenbo Guo[4]

[1]Institute of Geology and Geophysics, Chinese Academy of Sciences, Beijing 100029 E-mail: ppxueguoqiang@163.com, qqxueguoqiang@hotmail.com.

[2]Faculty of Science, International University of Africa, P.O.Box: 2469 Khartoum-SUDAN

[3]School of Geology and Survey, Chang'an University, Xi'an, China, 740064 E-mail:lixiu@chd.edu.cn.

[4]Geophysical and Geochemical Exploration Team, Northwest Geological Bureau for Non- ferrous Metals, Xi'an, China, 710068 E-mail: guowenbo@tom.com.

ABSTRACT

Electromagnetic geophysical methods include frequency-domain, plane-wave electromagnetic methods such as far-field, control source magnetotelluric (CSAMT) and magnetotelluric (MT) methods and time-domain methods such as loop-source transient electromagnetic method (TEM). Since TEM can easily get sounding data in near-zone and survey the whole response simultaneously, it has become widely used in engineering geology. However, compared to the well-established techniques for interpretation of the CSAMT and MT data, processing and interpretation of the TEM data are less developed. In this paper, based on a simple transformation relationship between measurement time and measurement frequency, we construct a method to transform the TEM sounding data into plane-wave electromagnetic sounding data. Because the propagation of electromagnetic waves and the seismic waves in a layered medium is similar, the plane-wave electromagnetic sounding data are further

transformed into seismic-like data, based on which the subsurface imaging is accomplished. A case study applying this new two-step conversion scheme is shown.

INTRODUCTION

Electromagnetic geophysical methods include frequency-domain methods such as MT and far-field CSAMT, which are usually regarded as wave field, and time-domain method (TEM), which belongs to diffusion field. The advantage of TEM over CSAMT and MT is that it can easily get sounding data in near-zone and simultaneously survey the whole response. However, the interpretation of TEM data is less developed than that of CSAMT and MT, particularly in imaging inversion.

Plane-wave electromagnetic (EM) fields have reflective and transmissive features during propagation, which are similar to the ways of seismic wave propagation. The similarity has been studied by Lee et al. (1989), who established an equation between the time-domain electromagnetic diffusion function and a pseudo-time-domain wave function, which would allow interpretation of electromagnetic data using pseudo-seismic methods. Further work was conducted by Lee and Xie (1993), Hoop (1996), Gershenson (1997), and Lee et al. (2002). However, such equations are difficult to solve as their inversions are ill-posed. The main difficulty with this technique is the size of matrix of equations. The study of EM migration in frequency-domain by Zhdanov (1993, 1996, 2006) is also based on the fact of the

similarity between diffusion field and wave field. The migration needs enormous amounts of computations.

Present Work

Subsurface imaging using magnetotelluric data was firstly accomplished by Levy et al. (1988), who derived the pseudo-impulse response from MT field data. Subsequent work by Levy et al. (1988) imaged MT data in one and two dimensions by using the linear programming method.

In order to correct the static shift of MT with TEM field data, the similar resistivity curves between MT sounding data and TEM sounding data have been discussed by Sternberg (1988), Meju (1996, 1998). The principle of the two kinds of fields has been analyzed by Raiche and Gallagher (1985).

If the plane-wave data can be transformed into data to which pseudo-seismic methods can be applied, then it provides an alternative method for interpretation of the plane-wave EM data. Similarly, if transient EM (TEM) data can be transformed into plane-wave data, then they also can be interpreted, in this way simplifying the interpretation.

Here we develop a means of transforming TEM sounding data into plane-wave sounding data that are further converted into seismic-like data. The resulting TEM pseudo-seismic data can be easily applied for subsurface imaging.

A similarity between MT and TEM sounding curves has been identified by Sternberg (1988) who used TEM sounding curves to correct the MT static shift. In converting measurement time to

measurement frequency, he used the empirical formulae: $\frac{194 \sim 200}{f} = t$.

We have undertaken a large number of forward calculations and statistically analyzed the results to derive a relationship between time and frequency. Based on this formula, the TEM sounding data can be transformed into plane-wave sounding data.

The plane-wave impedance can be calculated from the transformed plane-wave apparent resistivity and the reflection coefficient can be obtained from the calculated wave-impedance by linear-programming methods. During the inversion, in order to reduce the non-unique and unstable problem, linear programming method has been used.

Finally, an imaged section can be drawn using the reflection coefficient. The method has been tested on theoretical model data and field data with good results.

SIMILIARITY BETWEEN SEISMIC AND ELECTROMAGNETICS

In this section, we show the similarity between the equations governing electromagnetic waves and seismic waves. Then, we discuss the TEM and MT or CSAMT sounding curves and construct a factor to transform TEM sounding data into plane-wave sounding data.

The similarity between electromagnetic wave and seismic wave of a layered medium:-

Under the condition of a layered earth excited by a vertical incidence plane wave, the i-th electromagnetic field solution is:

$$E_x^i = D_i e^{-k_i z} + U_i e^{k_i z}, \qquad (1),$$

Levy et al., (1988)

$$H_y^i = -\frac{k_i}{i\omega\mu_0}(D_i e^{-k_i z} - U_i e^{k_i z}) \qquad (2)$$

where Di represents the up-wave, Ui represents the down wave (it would be more logical to swap these to make D down and U up). E_x^i is the electric field in the x direction, H_y^i is the magnetic field in the y direction. k_i is the wave number of the i-th layer, ω is circular frequency and $\mu_0 = 4\pi \times 10^{-7}\,\mathrm{H/m}$.

Applying the boundary conditions yields the plane wave-impedance [Levy et al., 1988]

$$Z_j(0, \omega) = Z_{01}(0, \omega) \left[1 + 2\sum_{m=1,}^{\infty} q_m e^{-2\sqrt{-i\omega t_0}\cdot m}\right] \qquad (3)$$

where m = 1, 2, 3……N, is the number of terms in the series.

j = 1, 2, 3……M, is the number of frequencies.

q_m is the reflection coefficients of the layered earth, and t_0 is the travel time of the electromagnetic wave.

In a layered earth, through which a vertical seismic wave is propagating, there is reflection. According to seismic wave theory, in the i-th medium:

$$U_i(z,\omega) = C_i \cdot e^{i\frac{\omega}{v_i}z} + G_i \cdot e^{-i\frac{\omega}{v_i}z}) \quad (4)$$

$$V_i(z,\omega) = \frac{1}{\rho_i \cdot v_i}(-G_i \cdot e^{-i\frac{\omega}{v_i}z} + C_i \cdot e^{i\frac{\omega}{v_i}z}) \quad (5)$$

where Ui and Vi are the force and velocity in the i-th medium at depth z, ρi·vi is the wave-impedance of the i-th medium, Ci represents the up wave and Gi represents the down wave.

Applying the boundary conditions and using equations (4) and (5) gives:

$$A = A_0\left[1 + 2\sum_{m=1}^{\infty} q_m^s e^{i2\omega m t_0}\right] \quad (6)$$

Where A is the ratio between force and velocity and A0 is the ratio at the surface of the ground. q_m^s is the reflection coefficients of seismic wave. It is clear that equations (3) and (6) have a similar form.

Using equation (3), we can obtain a reflection function qme at every survey point. This could be used to draw an electromagnetic response imaging section that is similar to a seismic time section.

Similarity between TEM and MT or CSAMT sounding curve

The rate that TEM fields diffuse is a function of the medium resistivity and the delay time. After the transmitter is switched off, the field decreases and diffuses into the underground medium. For a given depth, z, the secondary magnetic field component dB/dt will initially be zero, then, rises with time-delay, reaches a maximum and finally decays to zero. At time t the maximum electromagnetic field is at depth h'. The propagation velocity v and diffusion depth h' are related as follows (Raiche and Gallagher, 1985)

$$h' = \frac{2.898t}{(\pi\sigma\mu_0 t)^{1/2}} \qquad (7)$$

where σ is the conductivity of the medium.

This formula is similar to that derived to discuss the concepts of smoke rings

$$h = \frac{2.0t}{(\pi\sigma\mu_0 t)^{1/2}}, \qquad (8)$$

and also similar to the skin depth of a plane electromagnetic wave:

$$z = \sqrt{\frac{2}{\omega\mu_0\sigma}} = \sqrt{\frac{2}{2\pi f\mu_0\sigma}} \qquad (9)$$

The concept of skin depth and diffusion depth are related. In theory, seeing to any depth is possible at low frequencies or late time; but in practice, the depth of exploration depends on the instrument sensitivity, geo-electrical structure and the noise level. In favorable geological conditions, the practical depth of investigation may be several skin depths (or diffusion depths), whereas in complex geology

conditions, it may be much less than one skin depth (or diffusion depth).

When the geology is one dimensional, we assume that the skin depth and diffusion depth are equal

Let $h = z$ from (8) and (9), then:

$$\sqrt{\frac{2}{2\pi f \mu_0 \sigma}} = \frac{2.0t}{\sqrt{\pi \sigma \mu_0 t}} \qquad (10)$$

$$\text{then, } {}^{1}\!/_{\text{f}} = 4\text{t}, \qquad (11)$$

where the unit of t is second and the units of f is Hz.

When the unit of t is ms, the equation (11) can be written as:

$$f = {}^{250}\!/_{t} \qquad (12)$$

Using equation (7) instead of (8) and letting $\text{h}' = \text{z}$ gives:

$$\sqrt{\frac{2}{2\pi f \mu_0 \sigma}} = \frac{2.898\ t}{\sqrt{\pi \sigma \mu_0 t}}. \qquad (13)$$

$$\text{then, } {}^{1}\!/_{f} = 8.39t \qquad (14)$$

(for units of seconds and Hz), or

$$f = {}^{119.2}\!/_{t} \qquad (15)$$

(for units of ms and Hz). Obviously, there is some discrepancy in the magnitude of the scale factor.

In order to find a single scale factor in the transformation that is statistically good for most cases, we selected 20 scale factors in the transform. We list every scale factor from $\frac{150}{f} = t$ to $\frac{300}{f} = t$. Many

geo-electrical models have been forward calculated with TEM and CSAMT, then the time-frequency transformation of the two sounding curves has been undertaken for each scale factor. The discrepancy or error has been calculated and analyzed. The formula for calculating the error at each frequency is $\Delta\rho = \left|\frac{\rho_{CSAMT} - \rho_{TEM}}{\rho_{CSAMT}}\right| \times 100\%$ and the total relative errors is given by error=$\sum_{i=1}^{20} \Delta\rho_i$.

The results are shown in Figure 1 as a function of different scale factors for t= 0.087 to 7.0152 ms and f = 4096 to 1 Hz. The horizontal coordinate axis is the time shift relationship, and the vertical axis is the percent error. The minimum error occurs when using the equation $210/f = t$. In this case, the error is 5.85%. For the same time-frequency transformation, but a different time-delay and a different frequency, the error is different. In early-time or high frequency, the apparent resistivity errors are relatively large. The largest error is 31%, at late time or low frequency, the apparent resistivity error due to a poor time shift is relatively small. The smallest error is 0%.

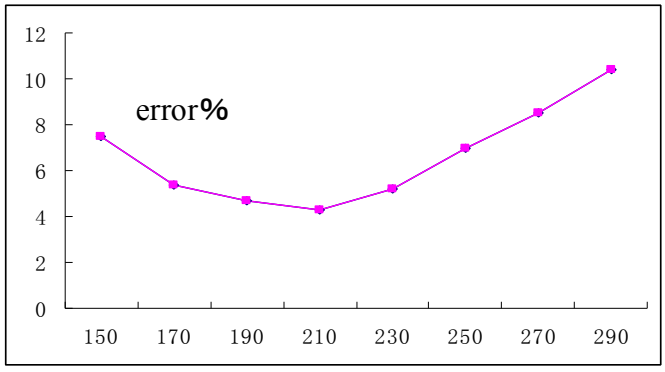

Fig. 1. Errors curve of every transformation factor

Our general conclusion is that the errors are smallest when the equation $210/f = t$ is used to transform between TEM field data and plane-wave field data.

In order to verify the exact relationship of the TEM and the plane wave resistivity sounding curve, we try to compare the geo-electrical models calculated using the TEM curve with the CSAMT curve. Figs. 2 and 4 show a D-type section ($\rho_1 = 100\Omega \cdot m$, $h_1 = 50m$, $\rho_2 = 25\Omega \cdot m$) and a G-type section ($\rho_1 = 25\Omega \cdot m, h_1 = 50m\ \rho_2 = 100\Omega \cdot m,$).

In the forward calculation, we assumed a CSAMT configuration. The adopted parameters are: I=10A, $r = 8000m$, $\theta = 90^\circ$ the range of transmitted and received frequencies are 4096 to 1 (Hz). According to the relationship between time and frequency: $t = 1/f$, the corresponding time range is 0.00024~1 s. In the forward calculation of the TEM data, the adopted parameters are: loop size L = 100m, transmitter current I = 10A. The range of sampling times are 0.087～7.0152 ms.

The shape of the two sounding curves is very similar in Figs. 2 and 4 where the frequency has been transformed by the factor: $t = 1/f$. Figs. 3 and 5 show the curves after the transformation by $210/f = t$. The curves virtually overlap after transformation.

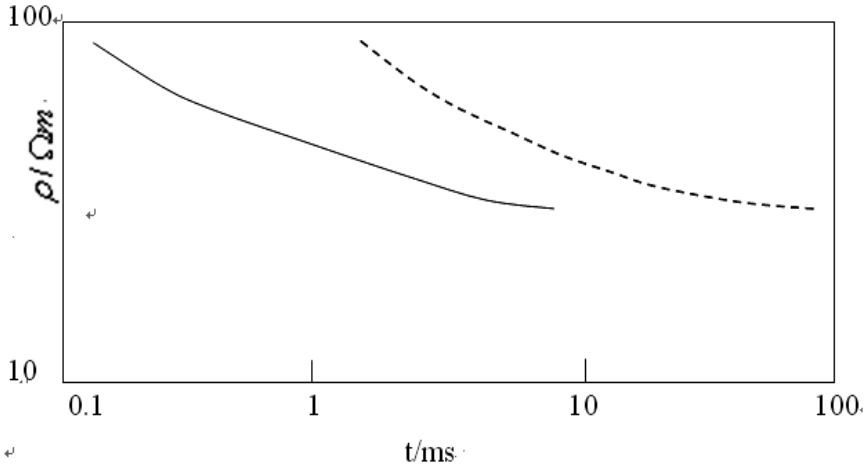

——— TEM data curve, ---: CSAMT data curve,

Fig. 2.Apparent-resistivity curve between CSAMT sounding and TEM sounding of D-type model before transform (the frequency of CSAMT curve has been transformed by $t=1/f$)

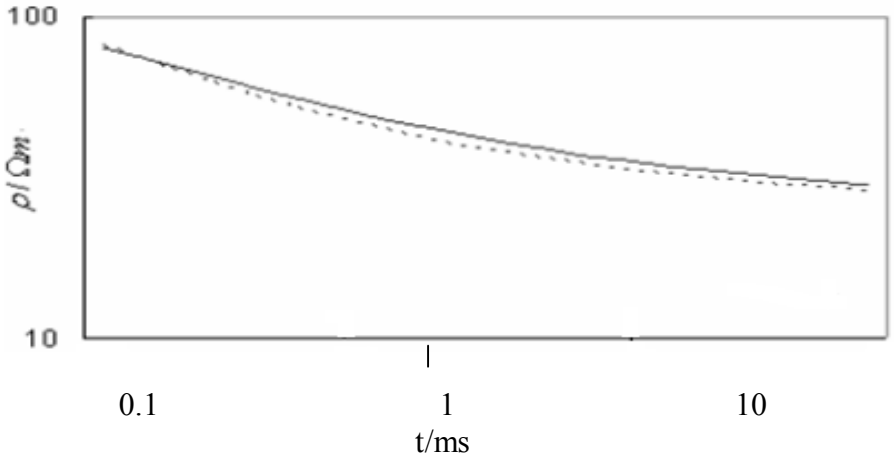

----------TEM ,——— CSAMT

Fig. 3 Apparent-resistivity curves of D-type after transformed with $210/f = t$ (the frequency of CSAMT curve has been transformed by $t = 210/f$)

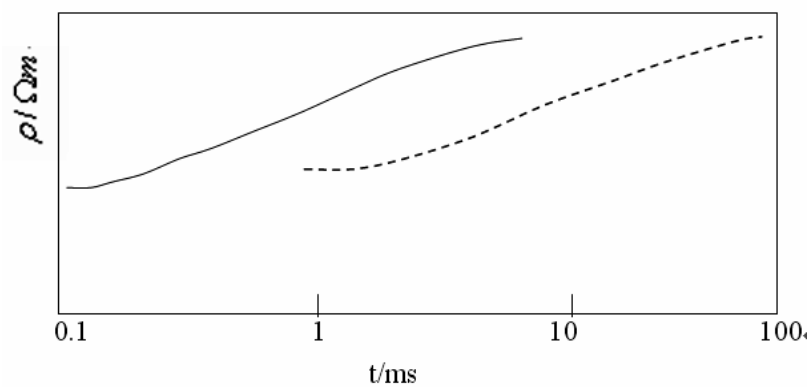

TEM data curve, ----- CSAMT data curve

Fig. 4 Apprent-resistivity curve of CSAMT sounding and TEM sounding of G-type (the frequency of CSAMT curve has been transformed by $t = 1/f$)

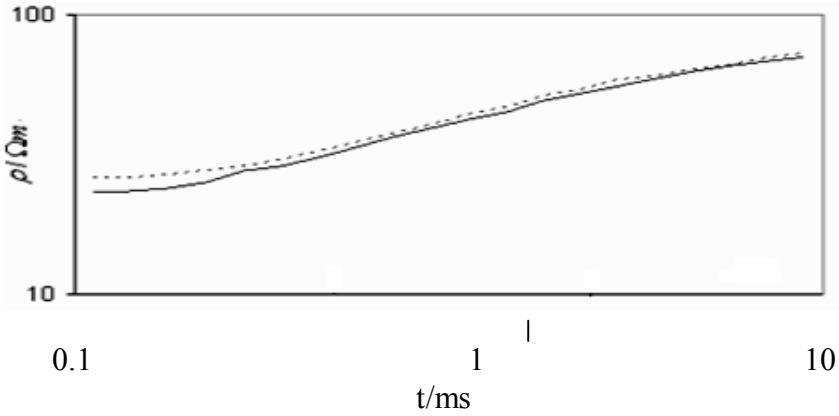

-------- CSAMT data curve, ----TEM data curve

Fig. 5 Apparent-resistivity curve between CSAMT sounding and TEM sounding of G-type model transformed with a factor of $210/f = t$ (the frequency of CSAMT curve has been transformed by $t = 210/f$)

TEM PSEUDO-SEISMIC IMAGING METHOD

After TEM sounding curves are transformed to equivalent plane-wave sounding curves, the final step is to form a pseudo-seismic imaging reflection function sequence q_m from the transformed data.

$$\text{Let } \mathrm{R}(\omega)=\frac{\dfrac{\mathrm{Z}(0,\omega)}{\mathrm{Z}_{01}(0,\omega)}-1}{2}\ , \tag{16}$$

then, (3) can be written as

$$\mathrm{R}_{\mathrm{j}}(\omega)=\sum_{m=1,}^{\infty} q_m^e e^{-2\sqrt{-i\omega t_0}\cdot m}\ . \tag{17}$$

where: j = 1, 2, 3……M, denotes the frequency number, Rewriting of equation (17) as a matrix equation, gives

$$\begin{cases} R_1 = P_{11}q_1 + P_{12}q_2 + \cdots + P_{1N}q_N \\ R_2 = P_{21}q_1 + P_{22}q_2 + \cdots + P_{2N}q_N \\ \vdots \quad \vdots \quad \vdots \quad \vdots \quad \vdots \\ R_M = P_{M1}q_1 + P_{M2}q_2 + \cdots + P_{MN}q_N \end{cases} \tag{18}$$

where: $p_{m,i} = -\dfrac{1}{2\pi i}\int \dfrac{e^{-2\sqrt{-i\omega_j t_0}\cdot m}}{\omega_j} e^{-i\omega_j t}\, d\omega$,

In order to obtain a reasonable solution of equation (10), we add a small error $\Delta \mathrm{R}_{\mathrm{j}}$, and then apply the following constraints :

$$\begin{cases} R_j + \Delta R_j \geq \sum_{m=1}^{N} q_m p_{m,j} \\ R_j - \Delta R_j \leq \sum_{m=1}^{N} q_m p_{m,j} \end{cases} \quad (19)$$

$$f_{\min} = |q_1| + |q_2| + \cdots + |q_N| \quad (20)$$

Where $\Delta R_j = 10$. The known variables are R_i and $P_{i,j}$, the unknown variables are $q_{m,}$ Solving for the unknowns with linear programming, yields the reflection coefficient sequence $q_{m,}$. Treating travel time as a depth coordinate, the q_m sequence can be plotted as a vertical section. This provides a straightforward way of visualizing the geo-electric structure.

APPLICATION AND RESULT

Using the method we propose in this paper, we processed theoretical models and TEM field data to produce an image section.

Theoretical modeling result :

We constructed two models (Q-type section, H-type section) and used these to generate theoretical data with the parameters I = 10A, L = 100m, and the time delays (t/ms): 0.087, 0.10961, 0.1381, 0.174, 0.21923, 0.2762, 0.348, 0.43845, 0.55242, 0.696, 0.87691, 1.1048, 1.392, 1.7538, 2.2097, 2.784, 3.507, 4.4193, 5.568 and 7.0152. For the CSAMT data, the frequencies are (f/Hz): 2873.56, 2293.58, 1811.6, 1436.79, 1141.55, 905.8, 718.39, 570.78, 452.9, 359.2,

285.39, 240.385, 179.6, 142.61, 113.17, 89.8, 71.29, 56.57, 44.9 and 35.64.

Figs. 6 and 9 are the apparent-resistivity curves between MT sounding and TEM sounding of Q-type and H-type model, respectively (the frequency of MT curve has been transformed by $t = 1/f$). Figs.7 and 10 are the apparent-resistivity curves between MT sounding and TEM sounding of Q-type and H-type model respectively (the frequency of MT curve has been transformed by $t = 210/f$). The two curves agree with each other after transformation.

The images are shown in Figs. 8 and 11. The electric interface can be clearly shown by a strong reflection coefficient. The time coordinate has been transformed to depth using the formula for the pseudo-time $t_0 = \mu_0 \sigma_1 h_1^2$ and velocity $V_i = \sqrt{\frac{2}{\mu_0 \sigma_i}}$.

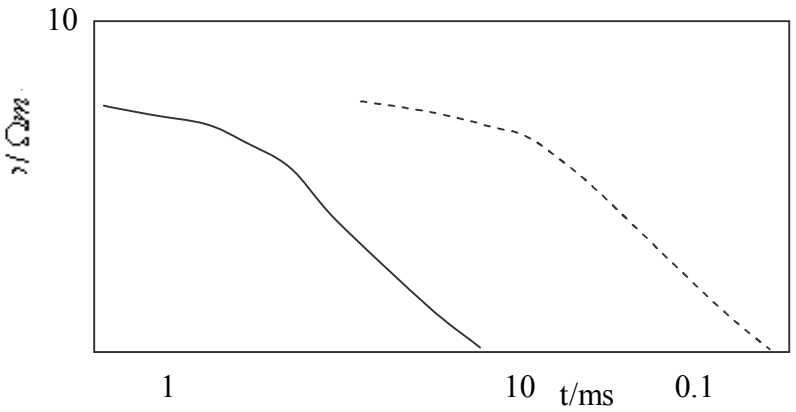

Fig. 6. TEM and MT forward calculation curve of Q-type section

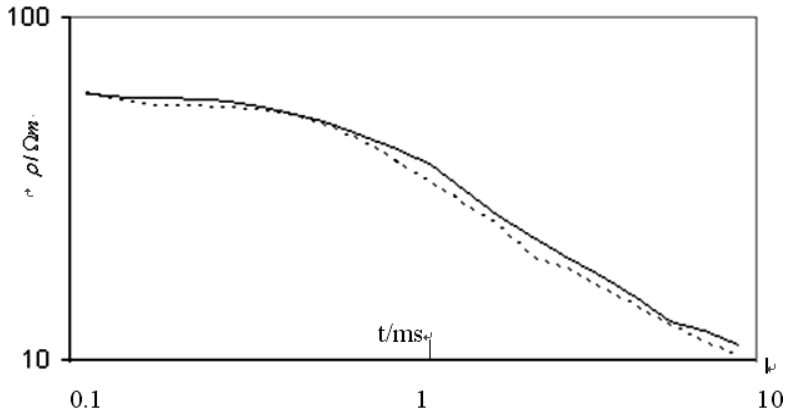

Fig. 7.TEM and MT forward calculation curve of Q-type section after

transformed with $210/f = t$ (the frequency of MT curve has been transformed by $t = 210/f$)

(1-MT data, 2-TEM data)

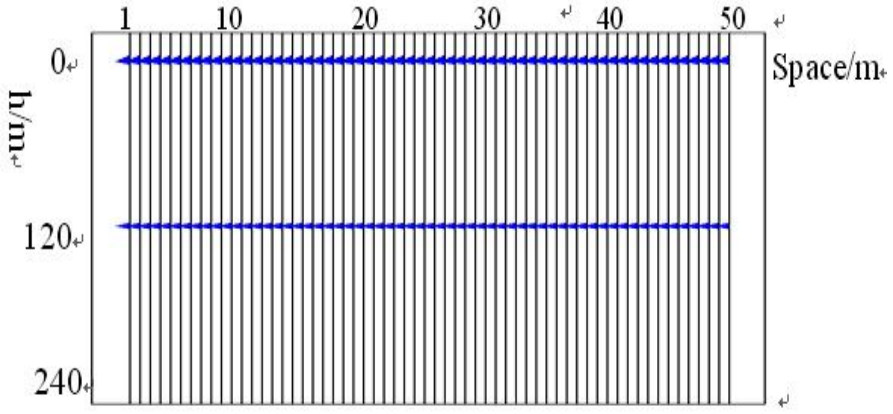

Fig. 8. Q-type imaging section

$(\rho_1 = 100\Omega \cdot m, \rho_2 = 36\Omega \cdot m, \rho_3 = 4\Omega \cdot m, h_1 = 20m, h_2 = 100m)$

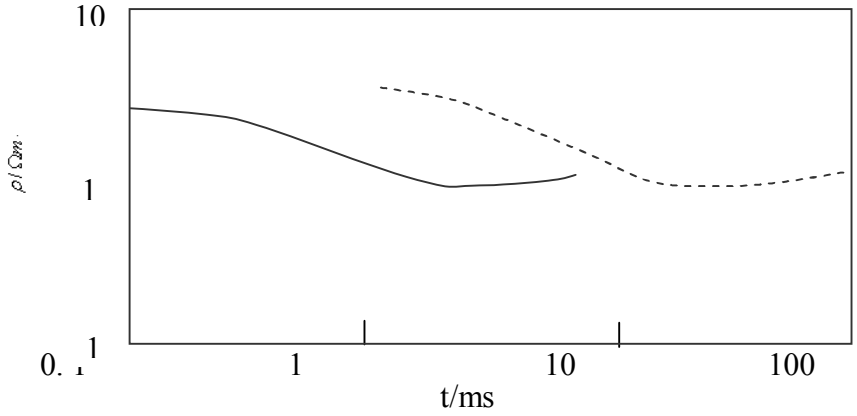

Fig. 9. TEM and MT forward calculation curve of H-type section

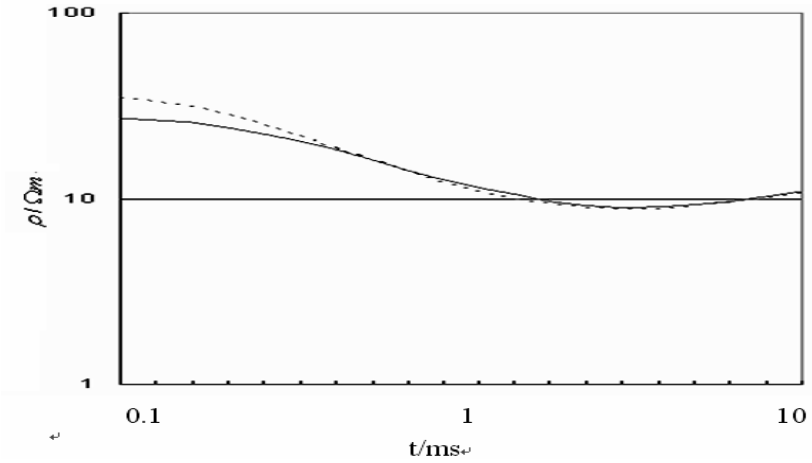

Fig. 10 Forward calculation curve (1-TEM curve, 2-MT curve)

after transformed with $210/f = t$ (the frequency of MT curve has been transformed by $t = 210/f$)

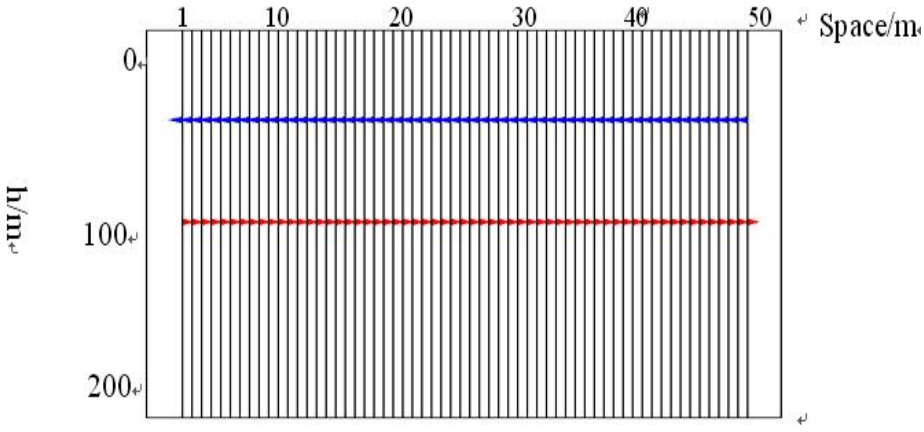

Fig. 11. H-type imaging section.

$$\rho_1 = 25\Omega \cdot m, \rho_2 = 4\Omega \cdot m, \rho_3 = 36\Omega \cdot m, h_1 = 10m, h_2 = 90m$$

The symbol σ_i denotes the first layer conductivity. These figures show clearly that the calculated depths agree with the given depths. Table 1 shows errors of reflection coeffiecent in the imaging parameter, the errors are less than 10%, which is a sufficient accuracy for estimating the depth when TEM is applied in engineering exploration.

In Table 1, the resisitivity of a specific layer can be obtained from $q_m = \dfrac{\sqrt{\rho_{m+1}} - \sqrt{\rho_m}}{\sqrt{\rho_{m+1}} + \sqrt{\rho_m}}$.

Table 1 Errors of reflection coefficients

model		Given value	Inversion result	error%
Q	q_1	-0.25	-0.243	2.8
	q_2	-0.5	-0.511	2.2
H	q_1	-0.429	-0.467	8.85
	q_2	-0.5	-0.489	2.2

Field Example

We used loop-source TEM to investigate an area where the station of current exchange of power transmission is planned by the government of Guangdong province, south China. In order to ground connect well the terminal transmission, the purpose is to identify the condition of engineering geology and to investigate the electric-distribution under the planned site. The configuration is a large rectangular loop. The instrument used is the SD-1.

Before the field work, there wais no geophysical data available, and we know little about the electric distribution in the investigated area.

The survey parameters were a transmitting loop 500m×500m and a receiver loop 20×20 m with 10 turns. The receiver was placed at the centre of the transmitter. The base frequency of the waveform was 6.25 Hz and the waveform was a square wave with a 0 ms turn off. The 20 time gates were placed between 0.216ms and 25.92ms after the switch off.

Fig. 12 is the TEM apparent resistivity contour section. In this figure, the values of apparent resistivity vary from top to bottom. We can not directly judge the electric interface, instead, we can only distinguish the electric distribution by our experience.

Fig. 13 is the imaging section. In the imaging calculation, near the point 6 and 14, two faults can be determined from the break of pseudo-seismic reflection coaxial and the electric distribution can be judged by the appearance of pseudo-seismic reflection coaxial. Because of the noise of the background, there exists discontinued or disappearance of the pseudo-seismic reflection coaxial in some surveying points, but the imaging result directly gives more geo-electric information than resistivity contour section.

Fig. 14 is an interpreted geological section showing the electric interface. There are four electric interfaces which separate the section into five electric layers. These layers are interpreted respectively as Quaternary System(Q), (rock type is clay), Cretaceous System(K), (rock type is red Conglomerate), Jurassic(J), (rock type Sandstone),Triassic(T) (rock type is Shale and mudstone,) and Carboniferous(C) (rock type is Sandstone and limestone) ,from top to bottom , with resistivity varying from $n\times 10^{1}$ to $n\times 10^{2}_{\times \Omega \cdot m}$. There are two faults in the point of 6 and 14. So, according to imaging section, we can distinguish underground electric distribution in the condition of little known basic geology information.

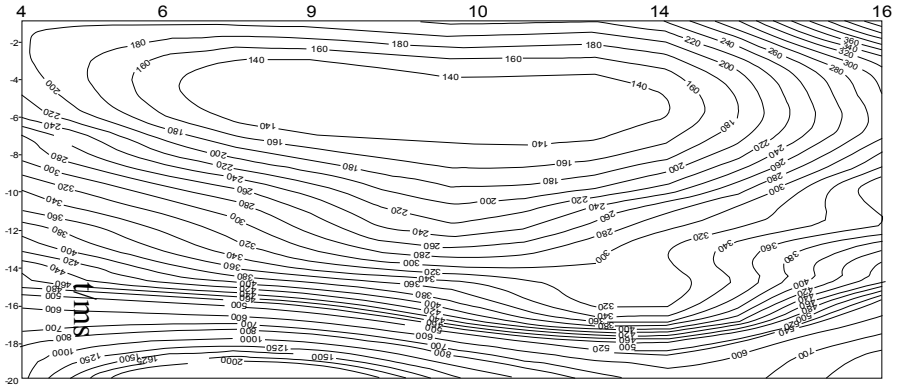

Fig. 12. Apparent-resistivity contour section

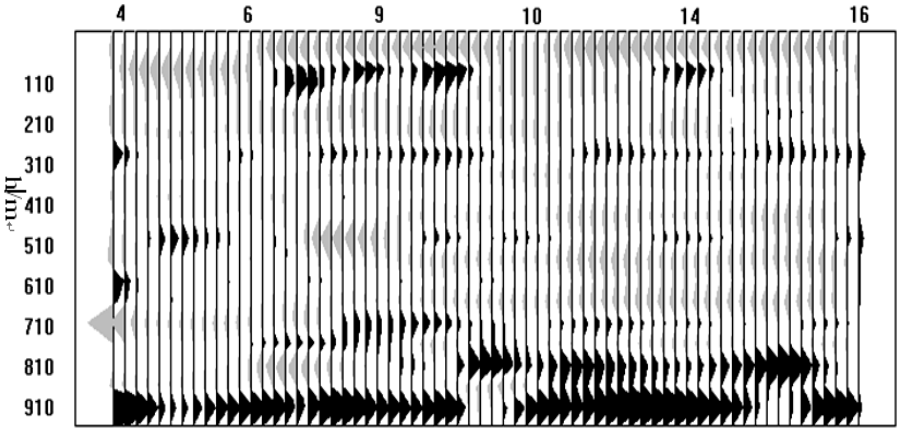

Fig. 13 Imaging section

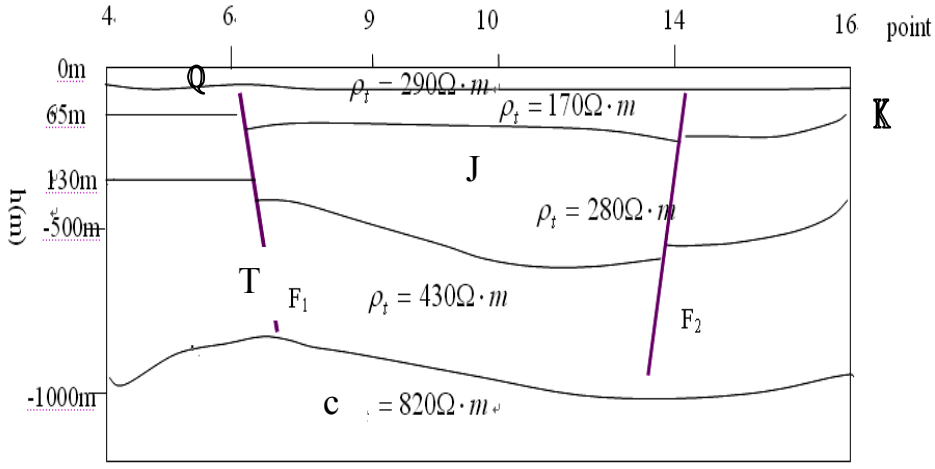

Fig. 14. Geoelectrical section. Q (Quqternary clay), K (Cretaceous – Red conglomerate), J (Jurassic Sandstone), T (Triassic Shale and Mudstone), C (Carboniferous Sandstone and Limestone).

DISCUSSION AND CONCLUSION

In order to improve the ability of transient EM methods to image the subsurface, we have proposed an imaging method exploiting a similarity between MT and TEM sounding curves, the TEM measurement time can be transformed into an equivalent frequency. The transformation factor is determined empirically from model data. TEM sounding data can be transformed into equivalent MT data through this time-frequency factor, then the TEM data can be imaged using an MT imaging method.

The imaging involves solving for the reflection coefficients at an electric interface using linear programming methods. The sequence of reflection coefficients are used to generate the section.

The section of TEM pseudo-seismic can directly distinguish the underground electric interface, especially in the case of poor geological information.

ACKNOWLEDGEMENTS

This work was supported by the National Nature Science foundation of China (40774066, 50539080).

References

Gershenson, M. (1997). Simple interpretation of time-domain electromagnetic sounding using similarities between wave and diffusion propagation. Geophysics, *62*, 763-774.

Hoop, A. T. (1996). Transient electromagnetic vs. seismic prospecting a correspondence principle. *Geophysical Prospecting*, *44*, 987-995

Lee, K. H., and G. A. Xie, (1993). New approach to imaging with low frequency electromagnetic field. Geophysics, *58*, 780-796.

Lee, K., H. G. Liu, and H. F. Morrison (1989), A New approach to modeling the electromagnetic response of condutive media. *Geophysics, 54*, 1180-1192.

Lee. T. J, J. H. Suh, H. J. Kim, Y. Song, and K. H. Lee. (2002). Electromagnetic travel time tomography using an approximate wave field transform. Geophysics*, 67*, 68-76.

Levy, S., D. Oldenburg, and J. Y. Wang (1988), Subsurface imaging using magnetotelluric data. *Geophysics, 53*, 104-117.

Meju, M. A. (1996), Joint inversion of TEM and distorted MT soundings, some effective practical considerations. *Geophysics, 61*, 56-65.

Meju, M. A. (1998), A simple method of transient electromagnetic data analysis. *Geophysics, 63*, 405-410.

Raiche A.P., and R. G. Gallagher (1985), Apparent resistivity and diffusion velocity. Geophysics*, 50*, 1628-1633.

Sternberg, B. K., J. C. Washburne, and L. Pellerin (1988). Correction for the static shift in magnetotellurics using transient electromagnetic sounding. *Geophysics, 53*, 1459-1468.

Zhdanov, M. S., and J. R. Booker (1993). Underground imaging by electromagnetic migration. The 63rd Ann. Internat. Mtg. Expl. Geophys. Expanded Abstr., 355-357.

Zhdanov M. S., P. Traynin, and J. Booker (1996). Underground imaging by frequency domain electromagnetic migration. Geophysic*s, 61*, 666-682.

Zhdanov, M. S. (2006). Iterative migration in marine CSEM data interpretation SEG/New Orleans 2006 annual Meeting, 810-813.